LIS1 is critical for axon integrity in adult mice

Abbreviated title: LIS1 iKO in adult mouse projection neurons

Samaneh Matoo, Anne M. Ventrone, Shreena Patel, Jack Otterson, Sean Noonan, Noah Leever, Ashley L. Kalinski, Deanna S. Smith

Department of Biological Sciences, University of South Carolina, Columbia, SC, USA, 29208

- ∴ Corresponding author email: deannasm@biol.sc.edu
- ∴ Number of pages
- ∴ Number of figures, tables, multimedia, and 3D models (separately)
- ∴ Number of words for abstract, introduction, and discussion (separately)
- ∴ The authors declare no conflicting financial interests
- ∴ Acknowledgments

Abstract

Mutations in LIS1 cause lissencephaly, a severe developmental brain malformation in humans. Altered proliferation and migration of neural precursors during brain development have been documented in mouse models. Although most studies focus on development, LIS1 is also expressed in adult mouse tissues. We previously induced LIS1 knockout (iKO) in adult mice using a Cre-Lox approach with an actin promoter driving CreERT2 expression. This proved to be rapidly lethal, but death occurred before tamoxifen-induced CreERT2 activity became widespread. The heart showed the highest level of CreERT2 activity, but heart-specific LIS1 depletion did not affect survival, ruling out a cardiac-based etiology. CreERT2 activity was observed in many astrocytes and some neurons in the brain suggesting that the defect could be related to defective cardiorespiratory circuits. We now report that LIS1 depletion from astrocytes is not lethal to mice although glial fibrillary protein (GFAP) expression is increased in LIS1 depleted astrocytes. In contrast, LIS1 depletion from projection neurons causes motor deficits and rapid lethality. This is accompanied by progressive, widespread axonal degeneration along the entire length of both motor and sensory axons. Interestingly, sensory neurons harvested from iKO mice initially extend axons in culture but soon develop axonal swellings and fragmentation, indicating axonal degeneration. LIS1 is a prominent regulator of cytoplasmic dynein 1, a microtubule motor whose disruption can cause both cortical malformations and later-onset neurodegenerative disease. Our results raise the possibility that LIS1 depletion, through disruption of dynein function in mature axons, may lead to Wallerian-like axon degeneration without traumatic nerve injury.

Significance Statement

A healthy nervous system requires that proper brain wiring is maintained throughout the life of the animal. Connectivity often involves the long axons of projection neurons. Some axons drive cognition, others contribute to sensory and motor systems, while still others subserve vitally important cardiorespiratory processes. We show that LIS1, a protein linked to congenital brain abnormalities, also plays a crucial role in fully developed projection neurons in the adult mouse. LIS1 depletion from these cells causes severe axonal degeneration resembling the Wallerian degeneration that occurs in response to nerve injury. Because LIS1 regulates dynein, and because defective dynein can cause neurodegenerative disorders in humans, our study suggests that drugs targeting Wallerian degeneration may have therapeutic potential for dynein related diseases.

Introduction

LIS1 mutations cause lissencephaly (smooth brain), an autosomal dominant disorder, with cognitive and motor impairments and short life expectancy (Di Donato et al., 2017; Brock et al., 2021). Germline knockout (KO) of *LIS1* in mice is peri-implantation lethal (Hirotsune et al., 1998). LIS1 binds to and regulates dynein, a microtubule (MT) motor(Faulkner et al., 2000; Liu et al., 2000; Smith et al., 2000); mutations in dynein heavy chain (*DYNC1H1*) also cause lissencephaly (Marzo et al., 2019; Moller et al., 2024). Defective dynein or reduced LIS1 interfere with the proliferation and migration of neural precursors, disrupting nuclear envelope breakdown, mitotic spindle dynamics, and nucleokinesis (Gambello et al., 2003; McManus et al., 2004; Wynshaw-Boris, 2007; Hebbar et al., 2008; Reiner and Sapir, 2013; Moon et al., 2014). LIS1 and dynein also contribute to phagocytosis in some cell types(Chhatre et al., 2020).

The proportion of active dynein motors in a cell is controlled by LIS1 (Baumbach et al., 2017; Gutierrez et al., 2017; Elshenawy et al., 2020; Markus et al., 2020; Marzo et al., 2020; Xiang and Qiu, 2020; Singh et al., 2024). Dynein exists in a closed, autoinhibited form (the *phi* conformation) or an open activatable form (Zhang et al., 2017). Only the open form associates with the dynactin complex and cargo adaptors, interactions that are required for processive movement. LIS1 prevents dynein from adopting the autoinhibited form, promotes transition to the open form, and promotes the recruitment of multiple motors per dynactin complex, increasing motor speeds and run lengths (Markus et al., 2020; Rao et al., 2025). LIS1 interacts with dynactin's p150 subunit, stabilizing dynein-dynactin complexes (Singh et al., 2024). These studies indicate that the proportion of dynein motors that are "activatable" as well as their speeds and run lengths can be influenced by local LIS1 concentration.

We showed that LIS1 also has post-developmental roles in mice. We used an actin promoter to drive a tamoxifen(TX) inducible CreERT2 recombinase globally in adult mice with heterozygous or homozygous floxed LIS1 alleles (Hines et al., 2018). Heterozygous iKO mice (TX-*Act-LIS1*$^{fl/wt}$) had no obvious neurological phenotypes and survived long term.

Despite widespread CreERT2 activity by two weeks. This indicated that loss of one LIS1 allele is well tolerated in adult mice. In contrast, homozygous deletion of LIS1 (TX-*Act-LIS1*$^{fl/fl}$) resulted in the rapid onset of severe neurological phenotypes, and mice died soon after TX administration. At peak phenotype severity the CreERT2 activity reporter showed prominent recombinase activity in the heart but only sparse activity in the nervous system and other tissues. A Myh6 promoter was used to drive CreERT2 in cardiomyocytes, but no phenotypes appeared, even long-term.

Within the nervous system, CreERT2 activity was predominantly observed in astrocytes and some neurons in the brainstem and hindbrain. We posited that defective cardiorespiratory and motor circuits might underlie the TX-*Act-LIS1*$^{fl/fl}$ phenotypes. Because LIS1 regulates key dynein-dependent processes in neurons, including long-distance cargo transport within axons (Sasaki et al., 2000; Yamada et al., 2008; Pandey and Smith, 2011; Yi et al., 2011; Pandey et al., 2022; Fellows et al., 2024) and the development and function of the axon initial segment (Kuijpers et al., 2016; Klinman et al., 2017; Torii et al., 2020) it seemed likely that at least some of the phenotypes were due to LIS1 depletion in neurons. However, many more astrocytes than neurons showed evidence of CreERT2 activation, raising the possibility these LIS1 depletion in astrocytes contributed to the iKO phenotypes. To determine the cell-type specific consequences of LIS1 depletion we have now used an Aldh1l1 promoter to drive CreERT2 expression in astrocytes (TX-*Aldh1l1-LIS1*$^{fl/fl}$ mice) and a Thy1 promoter to drive CreERT2expression in projection neurons (TX-*Thy1-LIS1*$^{fl/fl}$). The results unequivocally demonstrate a vital role for LIS1 in projection neurons and indicate that LIS1 depletion in these cells caused of the lethality in TX-*Act-LIS1*$^{fl/fl}$. Although LIS1 depletion in adult astrocytes did not produce obvious neurological symptoms or lethality, cellular changes suggest important roles for LIS1 in these cells.

Materials and Methods:

Animal Use

Animals were bred and housed at the University of South Carolina Animal Resources Facility. The following strains purchased from Jackson Laboratory were used to generate two iKO strains:

1*29S-Pafah1b1*^{tm2Awb}*/J*: (Jackson Laboratory 008002, RRID: IMSR_JAX:008002). Mice have loxP sites flanking exons 3–6 of the *Lis1* gene. This results in LIS1 depletion when mice are exposed to Tamoxifen (TX).

B6; FVB-Tg (Aldh1l1-cre/ERT2)1Khakh/J: (Jackson Laboratory 029655, RRID: IMSR_JAX:029655. Mice express a CreERT2 fusion protein in astrocytes. CreERT2 becomes activated and moves to the nucleus upon TX administration**.**

Tg (Thy1-cre/ERT2-EYFP) HGfng/PyngJ: (Jackson Laboratory 012708, RRID: IMSR_JAX:012708). Mice, also known as SLICK-H, express CreERT2 and enhanced yellow fluorescent protein (EYFP), each under the control of two separate modified Thy1 promoters. All projection neurons express EYFP. TX activates the CreERT2 in the same neurons.

B6. Gt(ROSA)26Sor*$^{tm9(CAG\text{-}tdTomato)\ Hze}$*/J: (Jackson Laboratory 007909, RRID: IMSR_JAX:007909): Mice, also known as Ai9, serve as a CreERT2 recombinase activity reporter; CreERT2 activity removes a loxP-flanked STOP cassette that prevents transcription of the CAG promoter-driven tdTomato. CreERT2 activity induced by TX results in robust tdTomato fluorescence. Genotyping of all animals was conducted using primers and protocols provided by The Jackson Laboratory, with primers available upon request. The designation for experimental and control animals used in the paper is shown in the following table, with the most commonly used controls being the no floxed LIS1 mice exposed to TX:

Nomenclature of most frequently used control and experimental animals:

	Astrocytes	**Proj. Neurons**
No floxed LIS1 controls	*TX-Aldh1l1-LIS1*$^{wt/wt}$	*TX-Thy1-LIS1*$^{wt/wt}$
No CreERT2 controls	*TX-LIS1*$^{fl/fl}$	*TX-LIS1*$^{fl/fl}$
No TX controls	*Aldh1l1-LIS1*$^{fl/fl}$	*Thy1-LIS1*$^{fl/fl}$
Experimental iKO mice	*TX-Aldh1l1-LIS1*$^{fl/fl}$	*TX-Thy1-LIS1*$^{fl/fl}$

Tamoxifen (TX) administration

Tamoxifen was administered to adult mice (aged 8-20 weeks) via intraperitoneal injections. For each injection, mice received 50 mg/kg body weight of TX (Sigma-Aldrich) dissolved in 100% corn oil (Sigma). Mice were usually given daily TX injections for five consecutive days, but in some experiments, this was reduced to injections for 3 consecutive days. "No TX" controls were given only vehicle (corn oil). All animal experiments were conducted under a protocol approved by the Institutional Animal Care and Use Committee (IACUC) of the University of South Carolina. Both male and female mice were included in the experiments, with no observed differences in outcomes between sexes.

Tissue Collection and Immunohistochemistry

Animals under deep isoflurane anesthesia were transcardially perfused with ice-cold PBS, followed by 4% paraformaldehyde (PFA) in 0.1 M PBS (pH 7.4). Tissue samples from the brain, spinal cord, and sciatic nerve were harvested and fixed in 4% PFA in PBS overnight. Tissues were then washed in phosphate buffered saline (PBS), cryoprotected in 30% w/v sucrose in PBS, embedded in Optimal Cutting Temperature Compound (O.C.T., Fisher) and stored at -80˚C. Tissues were cryo-sectioned at thicknesses ranging from 10 to 50 µm, and stored at −80°C. For immunostaining, sections were rehydrated in PBS, permeabilized with 0.3% Triton X-100 for 10–30 minutes, blocked with 10% goat serum, 3% BSA, and 0.1% Triton X-100 in PBS for 1 hour, then incubated with primary antibody overnight at 4°C. Primary antibodies used are as follows: LIS1 mouse monoclonal (Santa Cruz Biotechnology Cat# sc-17817, RRID:AB_627889; IF: 1:200, WB: 1:1000). NFL, NFM, and NFH, neurofilament light, medium, and heavy chain chicken polyclonals. Aves, RRIDs: AB_2313553, AB_2313554, AB_2313552; IF: 1:500); NF 200-kDa mouse monoclonal, clone RT97 (Millipore CBL212, RRID:AB_93408; IF: 1:500); Degenotag mouse monoclonal antibody to NF light chain (EnCor Biotechnology, Cat# MCA-1D44, RRID:AB_2923483; IF 1:1000); dynein intermediate chain mouse monoclonal (Santa Cruz Biotechnology sc-13524, RRID:AB_668849; IF: 1:200 WB: 1:1000) Vglut1 mouse monoclonal antibody (Invitrogen Cat # PIPA585764; IF: 1:250). GFAP mouse monoclonal antibody (Santa Cruz Biotechnology Cat # sc-33673, RRID:AB_627673; IF 1:1000, WB 1:500); After three PBS washes, sections were incubated for 2 hours with secondary antibodies (Alexa Fluor 555 or 647 conjugated, 1:500 dilution in PBS; Cy5-conjugated donkey anti-chicken, mouse, and goat (IF: 1:250; Jackson ImmunoResearch 703-175-155, 715-175-150, and 705-175-147, RRIDs:AB_2340365, AB_2340819, and AB_2340415). Nuclei were stained with Hoechst dye, and samples were mounted using Prolong Gold. Cryosections were imaged using a Leica STELLARIS 5 confocal microscope with LAS X software and a 20× or 63× oil immersion objective (1.4 N/A) or a Zeiss Axiovert 200 inverted microscope equipped with AxioVision software, a Plan-Neofluor 20× dry objective and Plan-Neo 100×/1.30 or Plan-Apo 63×/1.40 oil-immersion objectives (Immersol 518F; Carl Zeiss, Inc.)

C**ounting of axonal swellings and fragmentation in tissue sections, teased nerves and cultured neurons**

Axonal swellings were quantified in tissue sections and axons in DRG cultures. A swelling was counted if it had a diameter at least twice that of the associated axon. Swellings are labeled intensely with EYFP, probably due to accumulation. Fragmentation was determined for teased nerve preparations if the EYFP/tdTomato signal was broken along the length of the axons.

Fluoromyelin Staining

Tissues were rehydrated with PBS 3 times for 5 minutes each. Fluoromyelin red (Invitrogen, Cat# F34652) was diluted to 1X and applied for 20 minutes at room temperature. Tissues were rinsed 3 times for 5 minutes with PBS followed by one rinse with DI water. Tissues were air-dried at RT for 5 minutes and mounted with ProLong Gold antifade reagent with DAPI (Invitrogen, Cat# P36935). Tissues were imaged using a Zeiss AxioObserver 7 with an Apotome 3. Images were acquired with a Plan-Apochromat 20x/0.8 M27 air objective. 5 apotome images and optical sections at 0.2 um z step size were taken per field of view.

Protein isolation and immunoblotting

Tissues were rapidly dissected from CO2-euthanized mice and immediately frozen in liquid nitrogen, followed by homogenization using a Dounce homogenizer in ice-cold RIPA lysis buffer (50 mM Tris-HCl, pH 8.0, with 150 mM sodium chloride, 1.0% NP-40, 0.5% sodium deoxycholate, and 0.1% sodium dodecyl sulfate) containing HALT protease and phosphatase inhibitors (ThermoFisher, Cat# 78440). Protein concentrations in the extracts were quantified using a BCA assay (ThermoFisher, Cat# 33227). For Western blotting, 5 µg of Brain and spinal cord samples were separated on 4-15% acrylamide gels (BioRad, Cat # 4561084) and transferred to PVDF membranes. The blots were probed with

antibodies against LIS1 and dynein intermediate chain, with protein detection carried out via chemiluminescence. All blots are representative of at least three independent experiments.

Teased nerve preparation

Animals were deeply anesthetized with isoflurane and perfused transcardially with ice-cold PBS, followed by 4% PFA in 0.1 M PBS. The sciatic nerve was exposed by separating the biceps femoris along the intermuscular septum, then cut at the knee and sciatic notch before being fixed in 4% PFA overnight at 4°C. After post-fixation, a 3-5 mm nerve segment was trimmed and placed in PBS. Under a stereomicroscope, the epineurium was removed, and the nerve was teased into individual fibers on an adhesive slide. The slide was air-dried and stored at 4°C overnight before immunostaining the fibers for analysis.

Preparation of Astrocyte Cultures

Cultures were generated from iKO mice (TX-*Aldh1l1-LIS11* $^{fl/fl}$) and control mice TX-*Aldh1l1-LIS11* $^{wt/wt}$ or TX-*LIS1*$^{fl/fl)}$. Mice were euthanized on day 10 after the initial injection, then cortices removed and placed in cold Hanks Buffered Saline Solution (HBSS). After removing meninges and cutting cortices into small pieces, pieces were washed in HBSS 3 times and subjected to trypsin dissociation at 37˚C for 20 minutes. Cells were dissociated by trituration with a flamed Pasteur pipet, then incubated at 37˚C for 10 minutes. Cells were triturated again, then passed through a70 µm filter. Cells were pelleted by centrifugation at 8000 x g for 10 minutes. Pellets were resuspended in 10 mL of astrocyte media (DMEM/F12, 5% fetal bovine serum, 0.5% Non-essential Amino Acids and 0.5% penicillin-streptomycin), plated into T25 flasks, and maintained at 37˚C, 5% CO2. Medium was refreshed every 48 hours for 8 days, then cells placed on a shaker to shake at 37˚C for 2-4 hours to remove microglia. For imaging cells to were plated onto poly-D-lysine coated 12mm coverslips. Cells were fixed with 4% paraformaldehyde, processed for immunofluorescence, then mounted onto slides for confocal or widefield microscopy.

Preparation of DRG cultures

Mice were injected with TX in three daily doses. Dissociated cultures of adult DRG from iKO mice (TX-*Thy1-LIS1*$^{fl/fl}$) and control mice CreERT2 (TX-*LIS1*$^{fl/fl}$ or TX-*Thy1-LIS1*$^{wt/wt}$) were prepared as described by Twiss et al. (2000). DRGs were harvested in Hybernate A medium (ThermoFisher, Cat# A1247501) and dissociated using Collagenase type 2 (ThermoFisher, Cat#17101015) at 37°C with 5% CO2 for 15 minutes. DRGs were then triturated using a fire-polished Pasteur pipette, diluted in 5 ml DMEM/F12 (ThermoFisher, Cat#MT16405CV), and centrifuged at 100 x g for 5 minutes. After pelleting, dissociated DRGs were washed in DMEM/F12 and cultured in DMEM/F12 supplemented with 1x N1 supplement (Sigma, Cat#N6530), 10% fetal bovine serum (Hyclone, Cat#SH3007102), and 10 µM cytosine arabinoside (Sigma, Cat# C6645). The cells were plated on poly-L-lysine (ThermoFisher, Cat#A005C) and laminin (Sigma, Cat#CC095)-coated glass coverslips. After 72 hours, DRG cultures were harvested for immunostaining and imaging.

Experimental design and statistical analysis

Statistical tests and data graphing were performed using GraphPad Prism version 10. Individual animals were considered as biological replicates (*n*), and all experiments involve comparisons to littermate controls. The number of animals used (*n*), statistical measures represented in graphs, statistical tests performed, and *p* values are all reported in the legends. The threshold for statistical significance was defined as $p < 0.05$.

RESULTS

LIS1 depletion exclusively in astrocytes does not explain the phenotypes observed in TX-*Act-LIS1*$^{fl/fl}$ mice.

Astrocytes have important regulatory roles in the nervous system. They provide metabolic support to neurons, modulate synaptic function and maintain the blood brain barrier. Astrocytes also contribute to circuit remodeling by synapse phagocytosis(Chung et al., 2024). Dynein and LIS1 not only carry out cargo transport and regulate motility, they also contribute to phagocytosis (Chhatre et al., 2020; Omer et al., 2024). If LIS1 depletion disrupts these processes in adult astrocytes it could potentially lead to neurological impairment.

To ensure that LIS1 is expressed in adult astrocytes we examined dissociated cultured astrocytes using LIS1 immunofluorescence (IF). This allowed better separation of astrocytes from other cells in the brain. Astrocytes were harvested from adult mouse cortices and plated onto poly-D-lysine and laminin coated coverslips for staining and visualization. LIS1 displayed a typical punctate distribution with enrichment at centrosomes **(Fig 1 A)**. Dynein was also present in cultured astrocytes and enriched at centrosomes **(Fig 1B**). LIS1 was also frequently enriched around

what appear to be pyknotic nuclei that were likely phagocytosed from cells that died during the isolation procedure **(Fig 1 C, D).** This confirmed that LIS1 is present in adult astrocytes and may contribute to phagocytosis of cellular debris by astrocytes ((Chhatre et al., 2020; Lee et al., 2021).

To determine the importance of LIS1 expression in adult mouse astrocytes we used an *Aldh1l1* promoter to drive expression of CreERT2 specifically in astrocytes, generatingTX-*Aldh1l1-LIS1*$^{fl/fl}$ mice. These were crossed with a reporter strain that expresses tdTomato in cells with activated CreERT2 recombinase **(Fig 2 A)**. We used a standard IP injection TX dosing regimen, administering 50 mg/kg TX once a day for 5 days to both TX-*Aldh1l1-LIS1*$^{fl/fl}$ mice and TX-*ALDH1l1-LIS1*$^{wt/wt}$ controls **(Fig 2 A)**. Despite strong induction of tdTomato in all astrocytes by day 10 after the initial injection **(Fig 2 B)**, TX-*Aldh1l1-LIS1*$^{fl/fl}$ mice show none of the neurological impairments seen in the TX-*Act-LIS1*$^{fl/fl}$ mice (Hines et al., 2018). Astrocytes cultured from adult TX-*Aldh1l1-LIS1*$^{fl/fl}$ mice had reduced LIS1 expression **(Fig 2 C)** and displayed altered dynein distribution and MT organization suggestive of altered dynein activity in these cells **(Fig S1**). Because centrosomes are MT minus end hubs, less dynein at the centrosome, as observed in LIS1-depleted cells, supports that iKO astrocytes have less processive dynein motors **(Fig S1 A)**. There is substantial evidence that dynein contributes to MT organization in cells via MT sliding (Shima et al., 2006; Tanenbaum et al., 2013; Bender et al., 2015; Rao et al., 2017) so the altered MT distribution in LIS1-depleted astrocytes might reflect changes in MT sliding **(Fig S1 B).**

Despite these cellular changes, TX-*Aldh1l1-LIS1*$^{fl/fl}$ mice live normal life spans with no obvious neurological deficits such as leg clasping upon tail suspension **(Fig 2 D)**. However, astrocytes throughout the brain and spinal cord of TX-*Aldh1l1-LIS1*$^{fl/fl}$ displayed a strong increase in GFAP expression **(Fig 2 E, F)**. This was also observed in the TX-*Act-LIS1*$^{fl/fl}$ mouse model (Hines et al., 2018). Our new finding indicates that this is a cell autonomous response to LIS1 loss in astrocytes rather than a response triggered by alterations in neighboring LIS1-depleted neurons. Future studies will determine if loss of LIS1 in astrocytes produces more subtle behavioral consequences in mice due to the cellular changes in GFAP, dynein and MTs.

LIS1 depletion in projection neurons results in the rapid onset of neurological impairments and death

To determine the importance of lIS1 expression specifically in projection neurons we used the SLICK-H mouse strain to express CreERT2 (Vidal et al., 1990; Feng et al., 2000; Young et al., 2008). Expression of the recombinase and a separate allele of EYFP is controlled by two separate Thy1 promoters **(Fig 3A).** We used the same dosing regimen for these mice as with the TX-*Aldh1l1-LIS1* mice, 50 mg/kg TX once a day for 5 days **(Fig 3B)**. All projection neurons in SLICK-H mice are all labeled with EYFP, regardless of whether CreERT2 is activated by TX **(Fig 3 C** shows cortical pyramidal neurons). N either TX-*Thy1-LIS1*$^{wt/wt}$ control mice nor heterozygous iKO mice (TX-*Thy1-LIS1* $^{fl/wt}$) show any overt neurological phenotypes **(Movie 1)**. Homozygous iKO mice (TX-*Thy1-LIS1*$^{fl/fl}$), have reduced LIS1 expression compared to controls, bot by western blotting and IF **(Fig 3 D, E).** These mice displayed leg clasping upon tail suspension on day 6 after the first injection **(Fig 3 B, F)**. More severe symptoms became apparent between day 9 and 10 after the first injection **(Movie 2, Fig 3 B)**. Mice had an altered gait, exhibited severe shivering and "Straub tail" (a reaction caused by contraction of the sacrococcygenus muscle). There was also significant weight loss in the iKO mice. Homozygous iKO mice were routinely euthanized on day 10 after the initial TX injection.

LIS1 depletion in projection neurons results in axonal pathologies

Axons in *TX-Thy1-LIS1*$^{fl/fl}$ mice but not *TX-Thy1-LIS1*$^{wt/wt}$ controls developed axonal swellings by day 10 after the initial injection, as shown here in longitudinal spinal cord sections (**Fig. 4 A, B**). The number of swellings was significantly higher in *TX-Thy1-LIS1*$^{fl/fl}$ mice compared to controls **(Fig. 4 C)**. Additionally, the number of swellings in the spinal cord was progressive, being significantly higher on day 6 after the initial injection than on day 5, which correlates with the onset of neurological symptoms on day 6 **(Fig. 4 D)**. The swellings and fragmentation are reminiscent of the degeneration of axons distal to the site of a nerve injury (Wallerian degeneration). Similar axonal pathologies are also typical of most if not all neurodegenerative diseases, and indeed, may involve similar pathways that trigger programmed axonal death(Coleman and Hoke, 2020).

To definitively assess whether the fragmentation represents axon degeneration, we used the "Degenotag" antibody for immunofluorescence on spinal cord sections. This antibody has been used in the study of degenerative diseases and after nerve injury, as it allows visualization of neurofilament (NF) proteolysis by calpain and other proteases(Shaw et al., 2023). The Degenotag antibody recognizes a neurofilament light chain epitope not exposed until the protein is proteolytically cleaved. Spinal Cord sections from TX-*Thy1-LIS1*$^{fl/fl}$ mice exhibited substantially

higher Degenotag immunofluorescence than those from TX-*Thy1-LIS1*$^{wt/wt}$ controls, further confirming active axonal degeneration in the LIS1 depleted neurons **(Fig 4 E-G).** In Wallerian degeneration, the myelin sheath also breaks down in the nerve distal to the injury site(Conforti et al., 2014). To determine if there is myelin breakdown in sciatic nerve sections from TX-*Thy1-LIS1*$^{fl/fl}$ mice we used fluoromyelin staining **(Fig. 4H)**. There appears to be fragmentation and accumulation of myelin, supporting the idea that LIS1 depletion in projection neurons induces Wallerian-like degeneration. Future studies will be needed to determine if there is evidence of Schwann cell changes or macrophage invasion in nerves undergoing degeneration due to LIS1 depletion, as this is typical of Wallerian degeneration (Zhao et al., 2022). Because axons were degenerating in TX-*Thy1-LIS1*$^{fl/fl}$ mice, we reasoned that synapses may also be impacted. Indeed, VGLUT1 immunofluorescence revealed fewer synapses on the somatic motor neurons in the spinal cord ventral horns of TX-*Thy1-LIS1*$^{fl/fl}$ mice compared to controls on day 10 after initial TX exposure **(Fig. 4 I, J).** We have not detected apoptosis of LIS1 depleted neurons (not shown) indicating that LIS1 depletion triggers Wallerian-like axonal death without causing neurons themselves to die. Lowering the TX dose further to induce depletion in even fewer neurons may allow animals to survive even longer, allowing us to determine if neurons with degenerating axons eventually die.

Widespread neuronal Cre activation correlates with axon fragmentation in sciatic nerves of inTX-*Thy1-LIS1*$^{fl/fl}$ mice. *TX-Thy1-LIS1*$^{fl/fl}$ mice were crossed with the strain expressing the tdTomato Cre activity reporter **(Fig 5A).** Virtually all EYFP-positive neurons in the hippocampus of *TX-Thy1-LIS1*$^{fl/fl}$ mice also had tdTomato fluorescence by day 6 after the initial TX injection **(Fig. 5 B, C)** and this was true throughout the brain and spinal cord (not shown) as well as in peripheral nerves **(Fig 5D).** Control mice without Thy1-CreERT2 expression did not express tdTomato, other than an occasional cell, as indicated in the original paper describing these mice (Young et al., 2008). Axons labeled with both EYFP and tdTomato in teased sciatic nerve preparations from *TX-Thy1-LIS1*$^{fl/fl}$ mice, but not *TX-Thy1-LIS1*$^{wt/wt}$ controls, were often fragmented and showed swellings similar to those observed in spinal cord tissue sections (**Fig. 5 D, E).** Both sensory and motor axons developed swelling and fragmentation, as detected in teased nerve preparations of sural (sensory) and peroneal (motor) nerves **(Fig. 5 F)**.

***TX-Thy1-LIS1*$^{fl/fl}$ exhibit fewer neurological phenotypes after only 3 TX injections.** We tested 12 mice *TX-Thy1-LIS1*$^{fl/fl}$ sand 12 *TX-Thy1-LIS1*$^{wt/wt}$ controls with a lower TX dose by giving 3 consecutive daily TX injections instead of 5. After only 3 TX injections LIS1 iKO mice survived beyond day 10 and showed no shivering, seizures, or weight loss at that time **(Fig. 6 A, B)**. Upon examination of brain sections, it became clear that fewer neurons had activated CreERT2 in mice that only received 3 TX injections which likely explains the less severe phenotypes **(Fig. 6 C, D)**. Mice did exhibit leg clasping upon tail suspension on day 6 and began to have increased neurological symptoms. Mice were euthanized 22 days after the initial injections. Because animals survive longer with 3 injections, we were able compare axonal swelling on day 10 and day 22 in these mice. Interestingly there are significantly more swellings on day 22 after the initial injection **(Fig 6. E, F**). These findings indicate that there is a correlation between symptom severity and number of neurons with LIS1 loss. They also add support to the idea that LIS1 depletion initiates a progressive axonal degeneration process that continues to worsen over time, in that neurons with LIS1 depletion will continuously degenerate if the animal's survival is sustained by the unaffected neurons.

LIS1 depletion does not prevent axon growth in culture, but axons show signs of degeneration. Cultured DRG neurons from *TX-Thy1-LIS1*$^{fl/fl}$ animals exposed to 3 TX injections were able to extend long axons in culture despite showing reduced LIS1 staining, particularly in growth cones and axon shafts **(Fig. 7A).** They were also positive for Degenotag, indicating that despite axon extension, pathological changes to NF light chains were present. **(Fig. 7B)**. In addition, these axons appeared more fragile than controls and exhibited increased numbers of large varicosities **(Fig. 7C, D).** Together, these data suggest that LIS1 depletion allows axon extension but compromises axonal integrity.

DISCUSSION

This study establishes that LIS1 plays a critical role in maintaining the structural and functional integrity of projection neurons in the adult nervous system. We employed inducible knockout strategies to test this and found direct evidence that LIS1 depletion in projection neurons, but not in astrocytes, triggers rapid-onset axonal pathology, synaptic dysfunction, motor deficits, seizures, and premature lethality. These findings reveal an essential requirement for LIS1 specifically in adult mouse projection neurons and demonstrate that its role in regulating dynein

activity extends well beyond development into the long-term preservation of neuronal health and maintenance of neuronal function.

A central observation of our study is that LIS1 depletion in projection neurons induces axonal swellings, fragmentation and accumulation of neurofilament degradation products characteristic of the Wallerian degeneration that occurs in distal axons after axotomy. These degenerative changes were not restricted to distal axons, as would be typical in a "dying-back" model of neurodegeneration, but instead occurred along the entire axonal length. This suggests that LIS1 loss disrupts dynein-mediated axonal transport globally, impairing the ability of projection neurons to maintain axonal homeostasis. Given that projection neurons have exceptionally long axons and depend heavily on efficient bidirectional transport, even partial disruption of this system likely results in catastrophic structural instability. These findings align with prior studies showing that dynein dysfunction contributes to axonal degeneration in human motor neuron diseases such as Charcot-Marie-Tooth type 20 (CMT20) and spinal muscular atrophy with lower extremity predominance (SMALED).

Another important aspect of this work is the comparison of the phenotypes caused by LIS1 depletion in projection neurons and astrocytes. While neuron-specific LIS1 knockout led to severe neurological decline and death, astrocyte-specific LIS1 knockout produced no overt motor deficits or reduction in lifespan. The elevated GFAP expression observed in LIS1 depleted astrocytes is intriguing and demonstrates the functional significance of LIS1 in this cell type in adults. GFAP upregulation is a hallmark of "reactive astrogliosis" that occurs in response to stress, injury or inflammation in the CNS. By definition reactive astrogliosis is secondary to an extrinsic signal (Escartin et al., 2021). We did not intentionally provide an external signal so this LIS1 depletion response may not be classic reactive astrocytosis. However, if LIS1 loss in astrocytes perturbs their homeostatic roles in the brain, neurons may in fact develop pathologies and signal back to the astrocytes. Determining whether there is axonal degeneration in the astrocyte iKO mice will be an interesting future direction. Our early data indicate that LIS1 depletion in astrocytes impacts dynein distribution and microtubule trafficking (Fig. S1). It will be interesting to determine if astrocytic functions like phagocytosis and synaptic pruning are impacted by LIS1 depletion, and if astrocytic LIS1 depletion causes any behavioral changes in mice.

The graded effects of tamoxifen dosing allowed us to measure changes that occurred in axons over time. Mice receiving five consecutive tamoxifen injections displayed rapid, widespread and severe axonal degeneration. Animals needed to be euthanized by 10 days after the first injection, whereas mice exposed to fewer injections exhibited milder phenotypes and prolonged survival. This dose-dependent effect corresponds to the proportion of projection neurons undergoing recombination. Because of the complex cytoarchitecture and many cell types in the adult brain our finding underscores the importance of using a CreERT2 activity reporter to reveal which cells have undergone CreERT2 mediated recombination. The slower decline allowed us to determine that the pathological changes in individual axons became progressively worse with time.

Taken together, our findings suggest that LIS1 sustains neuronal viability in adulthood by supporting dynein-mediated transport and preventing activation of intrinsic degeneration pathways. Other processes known to involve LIS1 and dynein could also be affected and contribute to the phenotypes observed in TX-Thy1-LIS1fl/fl mice. Both LIS1 and dynein are important for the rerouting of misrouted dendritic components and the polarity sorting of microtubules at the AIS (Kuijpers et al., 2016; Klinman et al., 2017; Jenkins and Bender, 2024) and, although less well studied, LIS1 also functions in dendrites, at least during development (Kawabata et al., 2012; Sudarov et al., 2013). However, given the rapid onset of axonal degeneration, we consider disrupted axonal transport to be the most likely event contributing to the neurological phenotypes. Regardless, loss of LIS1 appears to tip the balance toward axonal self-destruction, with catastrophic consequences for neuronal and organismal survival.

Our results raise several new questions. First, does LIS1 serve as a protective factor against intrinsic degeneration programs? If so, does LIS1 perhaps do this by ensuring adequate delivery of metabolic substrates or structural components to distal axons? Does LIS1 depletion result in activation of known degenerative enzymes such as SARM1? In our earlier study with cultured rat DRG neurons knockdown of LIS1 (or expression of a dynein binding mutant) not only impacted retrograde organelle motility in axons but also perturbed anterograde motility, suggesting that LIS1 depletion could indeed impact delivery of important molecules into the axon (Pandey and Smith, 2011; Hines et al., 2018). Wallerian degeneration is triggered by the failed delivery of nicotinamide mononucleotide adenylyltransferase 2 (NMNAT2) into axons where it converts nicotinamide mononucleotide (NMN) and ATP to

NAD+(Gilley et al., 2015; Sasaki et al., 2016; Figley et al., 2021). The latter is critical for metabolic homeostasis, driving both mitochondrial function and on-board vesicle glycolysis during axonal transport. When NMNAT2 transport into axons is disrupted by injury, the buildup of NMN in axons stimulates a degeneration-associated NADase, SARM1 (Sterile alpha and TIR motif containing 1). SARM1 activation results in NAD+ depletion, ATP loss, and reduced mitochondrial motility and respiration (Ko et al., 2021). This latter causes calcium influx leading to membrane permeability, calpain activation and axonal fragmentation. If LIS1 activity is required for NMNAT2 delivery into axons its depletion could trigger the SARM1 degeneration pathway. LIS1 and SARM1 may therefore represent convergent points of regulation within shared axonal survival pathways, and therapeutic strategies aimed at modulating either protein could hold promise for neurodegenerative conditions involving dynein dysfunction. Dissecting whether LIS1 loss activates SARM1 directly or indirectly will be critical for developing targeted interventions. Finally, could modulation of LIS1 or its downstream pathways serve as a therapeutic strategy in disorders linked to dynein dysfunction, such as CMT20, SMALED, or even later-onset neurodegenerative diseases where axonal degeneration is a hallmark?

In conclusion, our findings establish that LIS1 is a vital regulator of neuronal survival well into adulthood. Its depletion leads to rapid axonal degeneration and neurological decline through mechanisms likely involving disrupted dynein activity. This work extends the functional scope of LIS1 beyond development, defining it as a lifelong guardian of axonal integrity in long-range projection neurons. This also provides new avenues for investigating therapeutic interventions aimed at preserving axonal health in neurodevelopmental and neurodegenerative disorders.

REFERENCES

Baumbach J, Murthy A, McClintock MA, Dix CI, Zalyte R, Hoang HT, Bullock SL (2017) Lissencephaly-1 is a context-dependent regulator of the human dynein complex. eLife 6.

Bender M, Thon JN, Ehrlicher AJ, Wu S, Mazutis L, Deschmann E, Sola-Visner M, Italiano JE, Hartwig JH (2015) Microtubule sliding drives proplatelet elongation and is dependent on cytoplasmic dynein. Blood 125:860-868.

Brock S, Dobyns WB, Jansen A (2021) PAFAH1B1-Related Lissencephaly / Subcortical Band Heterotopia. In: GeneReviews((R)) (Adam MP, Feldman J, Mirzaa GM, Pagon RA, Wallace SE, Amemiya A, eds). Seattle (WA).

Chhatre A, Sanghavi P, Mallik R (2020) Lis1 co-localizes with actin in the phagocytic cup and regulates phagocytosis. Cytoskeleton 77:249-260.

Chung WS, Baldwin KT, Allen NJ (2024) Astrocyte Regulation of Synapse Formation, Maturation, and Elimination. Cold Spring Harb Perspect Biol 16.

Coleman MP, Hoke A (2020) Programmed axon degeneration: from mouse to mechanism to medicine. Nature reviews Neuroscience 21:183-196.

Conforti L, Gilley J, Coleman MP (2014) Wallerian degeneration: an emerging axon death pathway linking injury and disease. Nature reviews Neuroscience 15:394-409.

Di Donato N, Chiari S, Mirzaa GM, Aldinger K, Parrini E, Olds C, Barkovich AJ, Guerrini R, Dobyns WB (2017) Lissencephaly: Expanded imaging and clinical classification. American journal of medical genetics Part A 173:1473-1488.

Elshenawy MM, Kusakci E, Volz S, Baumbach J, Bullock SL, Yildiz A (2020) Lis1 activates dynein motility by modulating its pairing with dynactin. Nature cell biology 22:570-578.

Escartin C et al. (2021) Reactive astrocyte nomenclature, definitions, and future directions. Nature neuroscience 24:312-325.

Faulkner NE, Dujardin DL, Tai CY, Vaughan KT, O'Connell CB, Wang Y, Vallee RB (2000) A role for the lissencephaly gene LIS1 in mitosis and cytoplasmic dynein function. Nature cell biology 2:784-791.

Fellows AD, Bruntraeger M, Burgold T, Bassett AR, Carter AP (2024) Dynein and dynactin move long-range but are delivered separately to the axon tip. The Journal of cell biology 223.
Feng G, Mellor RH, Bernstein M, Keller-Peck C, Nguyen QT, Wallace M, Nerbonne JM, Lichtman JW, Sanes JR (2000) Imaging neuronal subsets in transgenic mice expressing multiple spectral variants of GFP. Neuron 28:41-51.
Figley MD et al. (2021) SARM1 is a metabolic sensor activated by an increased NMN/NAD(+) ratio to trigger axon degeneration. Neuron 109:1118-1136 e1111.
Gambello MJ, Darling DL, Yingling J, Tanaka T, Gleeson JG, Wynshaw-Boris A (2003) Multiple dose-dependent effects of Lis1 on cerebral cortical development. J Neurosci 23:1719-1729.
Gilley J, Orsomando G, Nascimento-Ferreira I, Coleman MP (2015) Absence of SARM1 rescues development and survival of NMNAT2-deficient axons. Cell reports 10:1974-1981.
Gutierrez PA, Ackermann BE, Vershinin M, McKenney RJ (2017) Differential effects of the dynein-regulatory factor Lissencephaly-1 on processive dynein-dynactin motility. The Journal of biological chemistry 292:12245-12255.
Hebbar S, Mesngon MT, Guillotte AM, Desai B, Ayala R, Smith DS (2008) Lis1 and Ndel1 influence the timing of nuclear envelope breakdown in neural stem cells. The Journal of cell biology 182:1063-1071.
Hines TJ, Gao X, Sahu S, Lange MM, Turner JR, Twiss JL, Smith DS (2018) An Essential Postdevelopmental Role for Lis1 in Mice. eNeuro 5.
Hirotsune S, Fleck MW, Gambello MJ, Bix GJ, Chen A, Clark GD, Ledbetter DH, McBain CJ, Wynshaw-Boris A (1998) Graded reduction of Pafah1b1 (Lis1) activity results in neuronal migration defects and early embryonic lethality. Nature genetics 19:333-339.
Jenkins PM, Bender KJ (2024) Axon Initial Segment Structure and Function in Health and Disease. Physiol Rev.
Kawabata I, Kashiwagi Y, Obashi K, Ohkura M, Nakai J, Wynshaw-Boris A, Yanagawa Y, Okabe S (2012) LIS1-dependent retrograde translocation of excitatory synapses in developing interneuron dendrites. Nature communications 3:722.
Klinman E, Tokito M, Holzbaur ELF (2017) CDK5-dependent activation of dynein in the axon initial segment regulates polarized cargo transport in neurons. Traffic 18:808-824.
Ko KW, Devault L, Sasaki Y, Milbrandt J, DiAntonio A (2021) Live imaging reveals the cellular events downstream of SARM1 activation. eLife 10.
Kuijpers M, van de Willige D, Freal A, Chazeau A, Franker MA, Hofenk J, Rodrigues RJ, Kapitein LC, Akhmanova A, Jaarsma D, Hoogenraad CC (2016) Dynein Regulator NDEL1 Controls Polarized Cargo Transport at the Axon Initial Segment. Neuron 89:461-471.
Lee JH, Kim JY, Noh S, Lee H, Lee SY, Mun JY, Park H, Chung WS (2021) Astrocytes phagocytose adult hippocampal synapses for circuit homeostasis. Nature 590:612-617.
Liu Z, Steward R, Luo L (2000) Drosophila Lis1 is required for neuroblast proliferation, dendritic elaboration and axonal transport. Nature cell biology 2:776-783.
Markus SM, Marzo MG, McKenney RJ (2020) New insights into the mechanism of dynein motor regulation by lissencephaly-1. eLife 9.
Marzo MG, Griswold JM, Markus SM (2020) Pac1/LIS1 stabilizes an uninhibited conformation of dynein to coordinate its localization and activity. Nature cell biology 22:559-569.
Marzo MG, Griswold JM, Ruff KM, Buchmeier RE, Fees CP, Markus SM (2019) Molecular basis for dyneinopathies reveals insight into dynein regulation and dysfunction. eLife 8.
McManus MF, Nasrallah IM, Pancoast MM, Wynshaw-Boris A, Golden JA (2004) Lis1 is necessary for normal non-radial migration of inhibitory interneurons. The American journal of pathology 165:775-784.

Moller B et al. (2024) The expanding clinical and genetic spectrum of DYNC1H1-related disorders. Brain.
Moon HM, Youn YH, Pemble H, Yingling J, Wittmann T, Wynshaw-Boris A (2014) LIS1 controls mitosis and mitotic spindle organization via the LIS1-NDEL1-dynein complex. Human molecular genetics 23:449-466.
Omer S, Li J, Yang CX, Harrison RE (2024) Ninein promotes F-actin cup formation and inward phagosome movement during phagocytosis in macrophages. Molecular biology of the cell 35:ar26.
Pandey JP, Smith DS (2011) A Cdk5-dependent switch regulates Lis1/Ndel1/dynein-driven organelle transport in adult axons. J Neurosci 31:17207-17219.
Pandey JP, Shi L, Brebion RA, Smith DS (2022) LIS1 and NDEL1 Regulate Axonal Trafficking of Mitochondria in Mature Neurons. Front Mol Neurosci 15:841047.
Rao AN, Patil A, Black MM, Craig EM, Myers KA, Yeung HT, Baas PW (2017) Cytoplasmic Dynein Transports Axonal Microtubules in a Polarity-Sorting Manner. Cell reports 19:2210-2219.
Rao L, Liu X, Berger F, McKenney RJ, Arnold M, Stengel K, Sidoli S, Gennerich A (2025) The Power of Three: Dynactin associates with three dyneins under load for greater force production. bioRxiv.
Reiner O, Sapir T (2013) LIS1 functions in normal development and disease. Current opinion in neurobiology 23:951-956.
Sasaki S, Shionoya A, Ishida M, Gambello MJ, Yingling J, Wynshaw-Boris A, Hirotsune S (2000) A LIS1/NUDEL/cytoplasmic dynein heavy chain complex in the developing and adult nervous system. Neuron 28:681-696.
Sasaki Y, Nakagawa T, Mao X, DiAntonio A, Milbrandt J (2016) NMNAT1 inhibits axon degeneration via blockade of SARM1-mediated NAD(+) depletion. eLife 5.
Shaw G, Madorsky I, Li Y, Wang Y, Jorgensen M, Rana S, Fuller DD (2023) Uman-type neurofilament light antibodies are effective reagents for the imaging of neurodegeneration. Brain Commun 5:fcad067.
Shima T, Kon T, Imamula K, Ohkura R, Sutoh K (2006) Two modes of microtubule sliding driven by cytoplasmic dynein. Proceedings of the National Academy of Sciences of the United States of America 103:17736-17740.
Singh K, Lau CK, Manigrasso G, Gama JB, Gassmann R, Carter AP (2024) Molecular mechanism of dynein-dynactin complex assembly by LIS1. Science 383:eadk8544.
Smith DS, Niethammer M, Ayala R, Zhou Y, Gambello MJ, Wynshaw-Boris A, Tsai LH (2000) Regulation of cytoplasmic dynein behaviour and microtubule organization by mammalian Lis1. Nature cell biology 2:767-775.
Sudarov A, Gooden F, Tseng D, Gan WB, Ross ME (2013) Lis1 controls dynamics of neuronal filopodia and spines to impact synaptogenesis and social behaviour. EMBO molecular medicine 5:591-607.
Tanenbaum ME, Vale RD, McKenney RJ (2013) Cytoplasmic dynein crosslinks and slides anti-parallel microtubules using its two motor domains. eLife 2:e00943.
Torii T, Ogawa Y, Liu CH, Ho TS, Hamdan H, Wang CC, Oses-Prieto JA, Burlingame AL, Rasband MN (2020) NuMA1 promotes axon initial segment assembly through inhibition of endocytosis. The Journal of cell biology 219.
Vidal M, Morris R, Grosveld F, Spanopoulou E (1990) Tissue-specific control elements of the Thy-1 gene. The EMBO journal 9:833-840.
Wynshaw-Boris A (2007) Lissencephaly and LIS1: insights into the molecular mechanisms of neuronal migration and development. Clinical genetics 72:296-304.
Xiang X, Qiu R (2020) Cargo-Mediated Activation of Cytoplasmic Dynein in vivo. Front Cell Dev Biol 8:598952.

Yamada M, Toba S, Yoshida Y, Haratani K, Mori D, Yano Y, Mimori-Kiyosue Y, Nakamura T, Itoh K, Fushiki S, Setou M, Wynshaw-Boris A, Torisawa T, Toyoshima YY, Hirotsune S (2008) LIS1 and NDEL1 coordinate the plus-end-directed transport of cytoplasmic dynein. The EMBO journal 27:2471-2483.

Yi JY, Ori-McKenney KM, McKenney RJ, Vershinin M, Gross SP, Vallee RB (2011) High-resolution imaging reveals indirect coordination of opposite motors and a role for LIS1 in high-load axonal transport. The Journal of cell biology 195:193-201.

Young P, Qiu L, Wang D, Zhao S, Gross J, Feng G (2008) Single-neuron labeling with inducible Cre-mediated knockout in transgenic mice. Nature neuroscience 11:721-728.

Zhang K, Foster HE, Rondelet A, Lacey SE, Bahi-Buisson N, Bird AW, Carter AP (2017) Cryo-EM Reveals How Human Cytoplasmic Dynein Is Auto-inhibited and Activated. Cell 169:1303-1314 e1318.

Zhao XF, Huffman LD, Hafner H, Athaiya M, Finneran MC, Kalinski AL, Kohen R, Flynn C, Passino R, Johnson CN, Kohrman D, Kawaguchi R, Yang LJS, Twiss JL, Geschwind DH, Corfas G, Giger RJ (2022) The injured sciatic nerve atlas (iSNAT), insights into the cellular and molecular basis of neural tissue degeneration and regeneration. eLife 11.

FIGURE LEGENDS

Figure 1: LIS1 and dynein distribution in cultured adult mouse astrocytes. **A** LIS1 immunofluorescence (red) is prominent at the centrosome (arrow) near the nucleus (blue) in an interphase astrocyte also positive for GFAP (green). **B)** Dynein labeled with a dynein intermediate chain antibody is also enriched at a centrosome, here labeled with the centrosomal marker, pericentrin. **C)** LIS1 is enriched around an engulfed pynknotic nucleus (arrowhead). **D)** Pynknotic nuclei likely arise from neurons or other cell types that do not survive the dissociation process (arrows). In this image two healthy astrocyte nuclei are indicated with arrowheads. Scale bars = 10 µm.

Figure 2: TX-*Aldh1l1-LIS1$^{fl/fl}$* mice do not phenocopy TX-*Act-LIS1$^{fl/fl}$* mice, but astrocytes show elevated GFAP levels. A) Top diagram: Schematic of mouse crosses used to generate astrocyte specific iKO of LIS1 (*Aldh1l1-LIS1$^{fl/fl}$*). CreERT2 is a fusion of CreERT2 recombinase and a modified ligand-binding domain of the estrogen receptor, which is activated by the synthetic ligand tamoxifen (TX). CreERT2 mice are crossed with floxed LIS1 mice, where exons 3-6 of the LIS1 gene are flanked by LoxP sites and excised upon CreERT2 activation. Bottom diagram: TX is administered to adult mice (8-20 weeks old) at 50 mg/kg via IP injection for 5 consecutive days. **B)** tdTomato CreERT2 activity reporter is increased in astrocytes of in *TX- Aldh1l1-LIS1$^{fl/fl}$* mice. Scale bar = 25 µm. **C)** LIS1 expression (green) is reduced in astrocytes cultured from adult *TX- Aldh1l1-LIS1$^{fl/fl}$* mice compared to *TX- Aldh1l1-LIS1$^{wt/wt}$* control mice. Scale bar = 10µm. N≥3 culture preparations. **D)** *TX- Aldh1l1-LIS1$^{fl/fl}$* mice do not develop neurological impairments and survive at least 7 months after the first TX injection. **E)** Representative brain section stained with GFAP (green) and DAPI (blue), showing upregulation of GFAP expression in astrocytes of *TX- Aldh1l1-LIS1$^{fl/fl}$* mice. Scale bar = 10 µm. N≥ 4 mice per group. **F)** Western blot of brain tissue confirms increased GFAP expression in *TX- Aldh1l1-LIS1$^{fl/fl}$* mice. A Coomassie-stained gel shows equal protein loading.

Figure 3: TX-*Thy1-LIS1$^{fl/fl}$* mice have reduced LIS1 in fiber tracts and develop severe neurological symptoms. A) Schematic illustration of the generation of projection neuron specific conditional LIS1 knockout mice (TX-*Thy1-LIS1$^{fl/fl}$*). Two copies of the Thy1 promoter separately drive the expression of EYFP and the inducible CreERT2. **B)** The timeline of TX administration is similar to that of the TX-Aldh1l1-LIS1 mice, but iKO in projection neurons caused severe neurological symptoms and mice were euthanized on day 10 after the first injection. **C)** All projection neurons are labeled with EYFP (green) regardless of CreERT2 recombinase activity. Shown are labeled neurons in the cerebral cortex. Scale bar = 10 µm. The Zoomed shows clear EYFP signal in axons and cell bodies. **D)** EYFP-labeled axon tracts running in brainstem sections were processed for LIS1 immunofluorescence (magenta). The regions marked with an asterisk show that LIS1 expression is reduced in EYFP-labeled fiber tracts in *TX-Thy1-LIS1$^{fl/fl}$* mice compared to control *TX-Thy1-LIS$^{wt/wt}$* mice. The hashtags show that regions not positive for EYFP have substantial LIS1 labeling in both *TX-Thy1-LIS1$^{fl/fl}$* and *TX- Thy1-LIS$^{wt/wt}$* mice. Scale bar = 50 µm. N≥ 4 mice per group. **D)** Reduced LIS1 expression in *TX-Thy1-LIS1$^{fl/fl}$* mice (*fl/fl*) compared *TX-Thy1-LIS$^{wt/wt}$* mice (*wt/wt*) confirmed by western blotting of extracts from brain and spinal cord prepared on day 10. Levels of dynein intermediate chain (DIC) are not reduced and serve as a loading

control. **E)** On day 6 after the initial injection *TX-Thy1-LIS1*$^{fl/fl}$ mice exhibit neurological phenotypes such as leg clasping upon tail suspension, shown here.

Figure 4: LIS1 depletion in projection neurons causes axonal degeneration and synapse loss. A, B) Representative images of EYFP-positive axons in frozen longitudinal spinal cord sections from control mice *(LIS1*$^{wt/wt}$; left) and iKO mice (*LIS1*$^{fl/fl}$; right) mice treated with 5 doses of TX and perfused on day 10 after the initial injection. Axonal swellings (red arrows) are apparent in the *LIS1*$^{fl/fl}$ spinal cord. Scale bar = 50 µm. n $\geq$ 6 mice per group. **C)** Significantly more varicosities per mm² are present on day 10 *LIS1*$^{fl/fl}$ spinal cords compared to control *LIS1*$^{wt/wt}$ spinal cords. Graph shows the mean ± 95% CI. Significance determined by two-tailed Student's t test for 7 biological replicates. **D)** Varicosities are more prevalent in *LIS1*$^{fl/fl}$ spinal cord on day 6 than on day 5 after the initial injection per 0.3 mm² in *TX-Thy1-* after 5 TX doses and perfusion on days 5 and 6. n $\geq$ 3 mice per group. **E-G)** Representative images of EYFP + Degenotag immunofluorescence staining in longitudinal spinal cord sections from control *TX- Thy1-LIS*$^{wt/wt}$ (left) and *TX- Thy1-LIS1*$^{fl/fl}$ (right) mice perfused on day 10. Scale bar = 50 µm. Graph shows the mean ± 95% C. Significance determined by two-tailed Student's t test two biological replicates, 8 regions per tissue section. **H)** Myelin labeled with fluoromyelin in TX-*Thy1-LIS1*$^{fl/fl}$ sciatic nerve section appears fragmented and has accumulated in some regions (asterisks) but does not always correlate with sites of EYFP accumulation in axons (arrow). Scale bar = 25µm. **(I, J)** Synapses in the spinal cord ventral horn labeled with VGLUT1 (red) in TX-*Thy1-LIS1*$^{fl/fl}$ mice. A reduction in VGLUT1-labeled synapses was observed, suggesting that LIS1 depletion may disrupt synaptic integrity, potentially secondary to axonal degeneration. Quantification shows the number of VGLUT1 puncta per 100 µm. Graph shows the mean ± 95% C for 3 biological replicates 3 sections per mouse. Scale bar = 40 µm. Significance determined by two-tailed Student's t test.

Figure 5: Axonal degenerative profiles correlate with CreERT2 activity. A) Thy1-CreERT2 mice (both with and without floxed LIS1 alleles) were crossed with the tdTomato Cre activity reporter strain. **B)** tdTomato-positive neurons overlap substantially with EYFP positive neurons in the hippocampus on day 10 after the initial TX injection. Scale bars = 10 µm. **C)** The percent overlap was statistically significant compared to no-CreERT2 controls which had a very small number of tdTomato positive cells even in the absence of TX. Graph shows the mean ± 95% C for 3 biological replicates, 3 sections per mouse. Significance determined by two-tailed Student's t test. **D, E)** Individual axons in teased sciatic nerves are readily distinguishable and labeled with both EYFP and tdTomato. Only axons from TX-*Thy1-LIS1*$^{fl/fl}$ nerves showed significant levels of fragmentation. Graph shows the mean ± 95% C for 2 biological replicates, 4 regions of the teased nerve per sample. Significance determined by two-tailed Student's t test. **F)** Axons in teased nerve preparations from the sural (sensory) and peroneal (motor) nerves of *TX-Thy1-LIS1*$^{fl/fl}$ mice show axonal fragmentation. Scale bars = 50 µm; Scale bar in zoomed images in D = 100µm.

Figure 6: Fewer TX injections activate CreERT2 recombinase in fewer neurons resulting in fewer symptoms and delayed death. A) We compared the effects of giving 3 or 5 daily TX injections to TX-*Thy1-LIS1*$^{fl/fl}$ and TX-*Thy1-LIS1*$^{wt/wt}$ mice. Phenotypes were assay on days 6, 10 and 22 after the first injection. All TX-*Thy1-LIS1*$^{fl/f}$ that received 5 injections were euthanized on day 10 after the first injection. **B)** The number of mice that displayed the indicated symptom is shown for each genotype. Seizures and weight loss were only observed in TX-*Thy1-LIS1*$^{fl/f}$ mice that received 5 injections. *TX-Thy1-LIS1*$^{fl/f}$ mice that received only 3 injections had the leg clasping phenotype, but survived for 22 days, at which time they were euthanized. **C)** After only 3 injections fewer neurons in the cortex on day 10 after the initial injection were positive for the tdTomato CreERT2 activity reporter. Scale bar = 100 µm. **D)** Graph shows mean ± 95% CI for five biological replicates. Significance determined using ordinary one way ANOVA with multiple comparisons. **E, F**) Axons in TX-*Thy1-LIS1*$^{fl/fl}$ mice that received 3 days of TX also showed degenerative swellings, and the number increased between day 10 and 22 after the first injection. Scale bar = 50 µm. **F)** Quantitation of varicosities per mm² in the spinal cord on day 10 or day 22 after the first injection Graph shows mean ± 95% CI for three biological replicates $\geq$ 2 sections per animal. Significance determined using a two-tailed Student's t test.

Figure 7: LIS1 depletion does not prevent axon growth in culture, but axons show signs of degeneration. A) Representative immunofluorescence images showing tdTomato-labeled axon (Red)) + LIS1 staining (Cell body in grey and axon in royal blue) in cultured DRG neurons from *TX- Thy1-LIS1*$^{wt/wt}$ and *TX- Thy1-LIS1*$^{fl/fl}$ mice received five doses of TX. Axons from *TX- Thy1-LIS1*$^{fl/fl}$ mice have greatly reduced LIS1 protein levels compared to control axons. Graph shows mean ± 95% CI for 3 biological replicates, 20 axons per group. Significance determined using a two-tailed Student's t test. Scale bar = 20 µm. **B)** Cultured DRG neurons from *TX-Thy1-LIS1*$^{wt/wt}$ and *TX-Thy1-LIS1*$^{fl/fl}$ mice

received five doses of TX and were stained with Degenotag (cyan) to visualize degenerating axons. Scale bar = 10 µm. **C, D)** In cultured DRG neurons, axons from *TX-Thy1-LIS1*$^{fl/fl}$ mice appeared more fragile and fragmented than controls and exhibited a significant inCreERT2 in swellings per neuron, consistent with axonal pathology. The graph shows the mean ± 95% CI of neurons from 3 mice per genotype. Significance was determined by two-tailed Student's t test of measurements from 22 neurons per group. Scale bar= 10 µm.

Figure S1: LIS1 depletion in astrocytes results in altered distribution of both dynein and microtubules. A) Dynein immunofluorescence was visualized in cultured astrocytes using an antibody to dynein intermediate chains. Scale bar = 20 µm. **B)** The intensity of dynein at the centrosome in an area of consistent size was measured for 30 cells for each group in cultures from 3 biological replicates. Significance determined by two-tailed Student's t test; graphs show the mean ± 95% CI. **C)** Tubulin immunofluorescence was visualized in cultured astrocytes using an antibody to alpha-tubulin. Scale bar = 20 µm. **D)** A segmented line tool was used to measure the intensity of tubulin staining around 60 nuclei per treatment from 3 biological replicates. Significance determined by two-tailed Student's t test; graphs show the mean ± 95% CI**.**

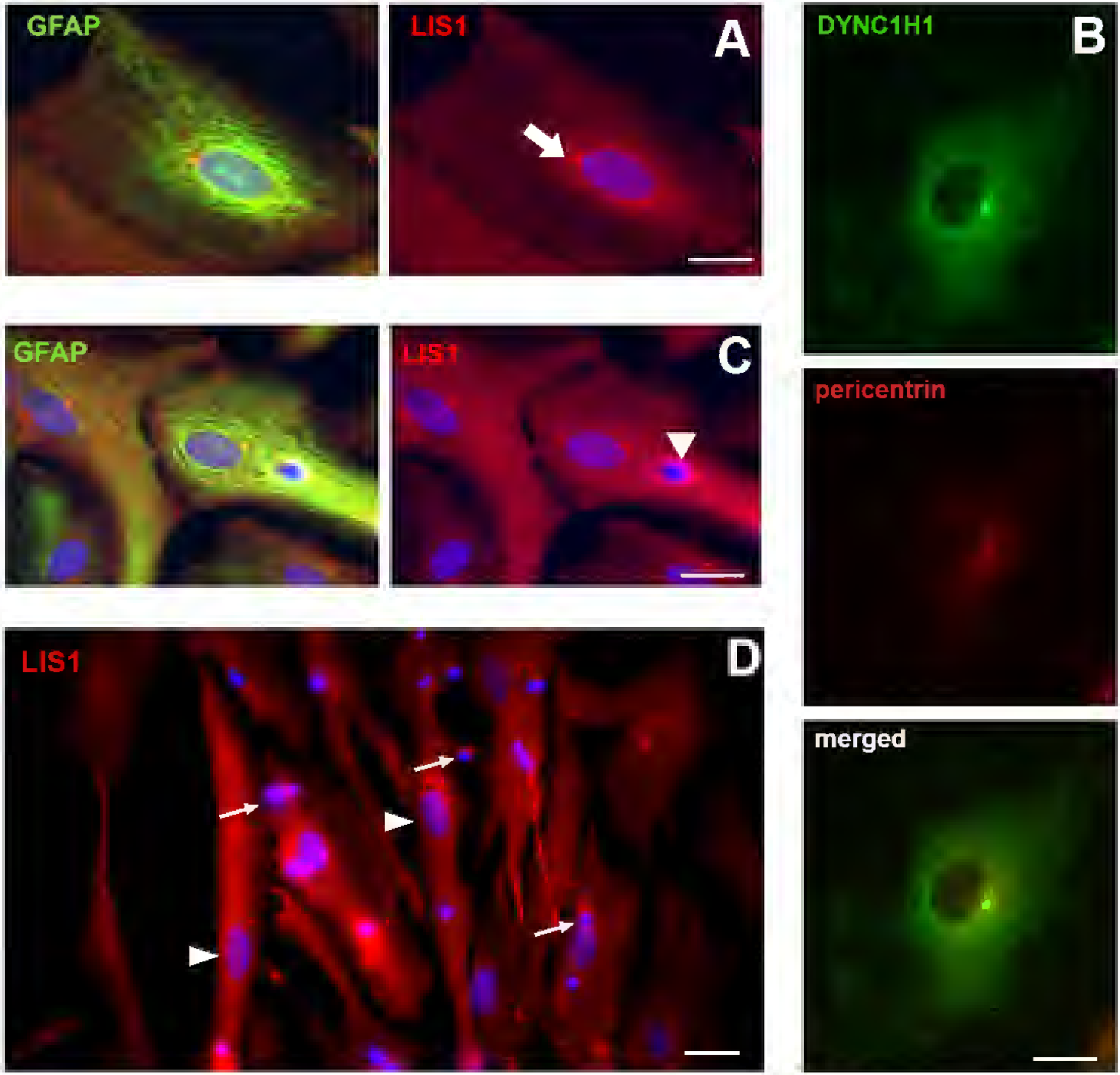
GFAP
LIS1
A
DYNC1H1
B
GFAP
LIS1
C
pericentrin
LIS1
D
merged

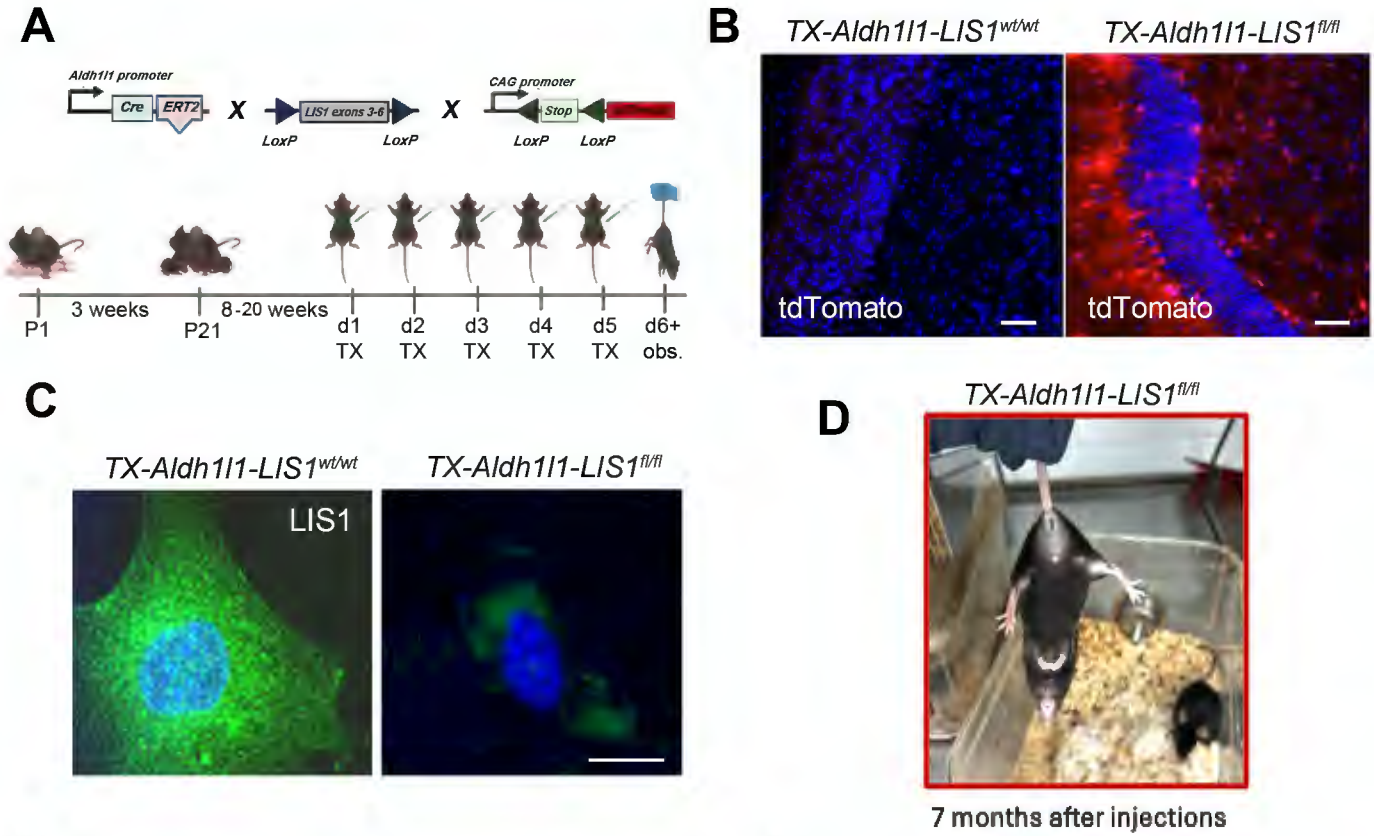
A
Aldh1l1 promoter
Cre
ERT2
X
LIS1 exons 3-6
LoxP
LoxP
X
CAG promoter
Stop
LoxP
LoxP
P1
3 weeks
P21
8-20 weeks
d1 TX
d2 TX
d3 TX
d4 TX
d5 TX
d6+ obs.
B
TX-Aldh1l1-LIS1wt/wt
TX-Aldh1l1-LIS1fl/fl
tdTomato
tdTomato
C
TX-Aldh1l1-LIS1wt/wt
TX-Aldh1l1-LIS1fl/fl
LIS1
D
TX-Aldh1l1-LIS1fl/fl
7 months after injections
E
TX-Aldh1l1-LIS1wt/wt
TX-Aldh1l1-LIS1fl/fl
GFAP
GFAP
F
Coomassie
GFAP WB
100-
75-
50-
37-
20-
wt/wt
fl/fl
100-
75-
50-
37-
20-
wt/wt
fl/fl

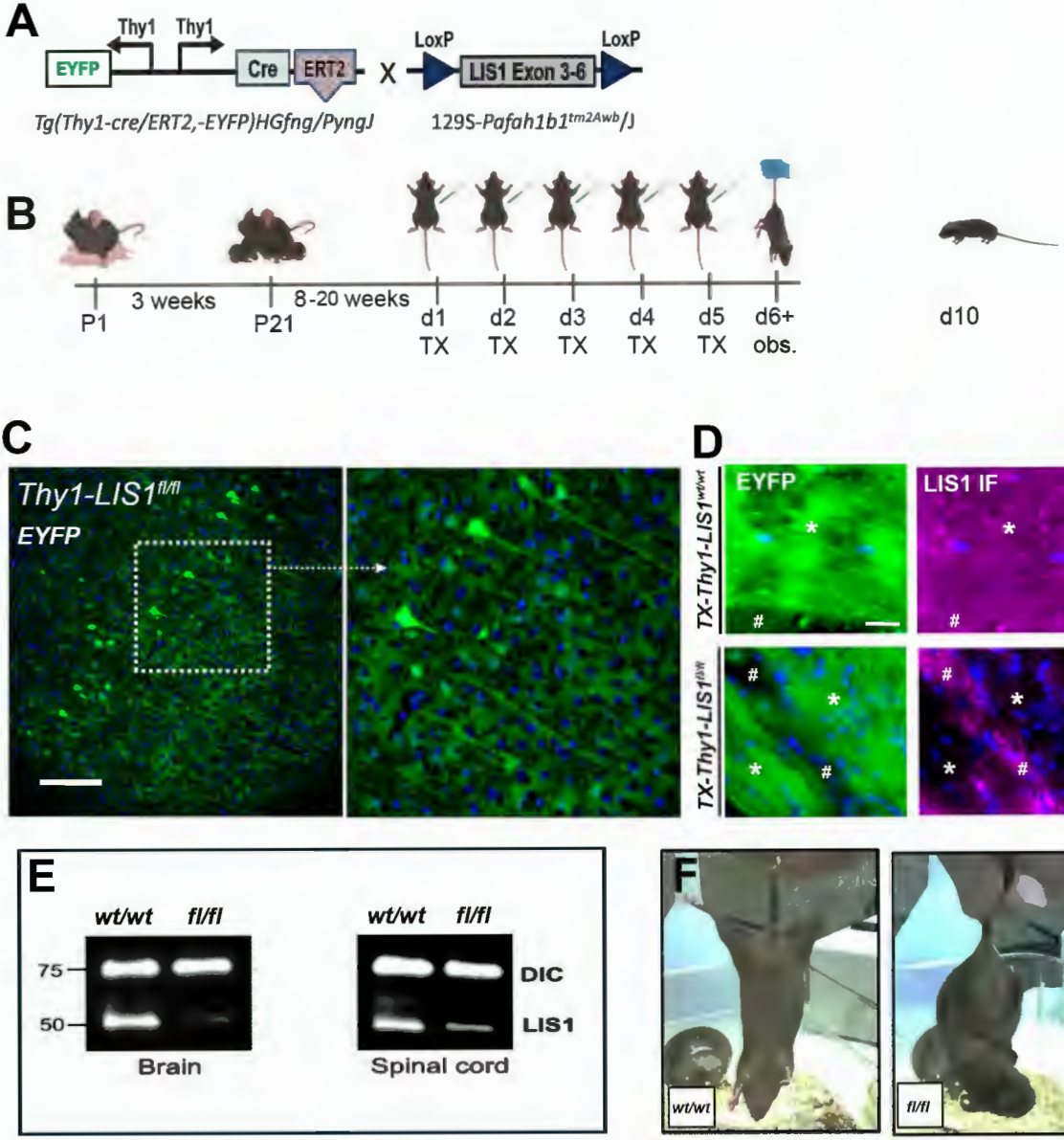
A
Thy1
Thy1
EYFP
Cre
ERT2
X
LoxP
LIS1 Exon 3-6
LoxP
Tg(Thy1-cre/ERT2,-EYFP)HGfng/PyngJ
129S-Pafah1b1tm2Awb/J
B
P1
3 weeks
P21
8-20 weeks
d1 TX
d2 TX
d3 TX
d4 TX
d5 TX
d6+ obs.
d10
C
Thy1-LIS1fl/fl
EYFP
D
EYFP
LIS1 IF
TX-Thy1-LIS1wt/wt
TX-Thy1-LIS1fl/fl
E
wt/wt
fl/fl
75
50
Brain
wt/wt
fl/fl
DIC
LIS1
Spinal cord
F
wt/wt
fl/fl

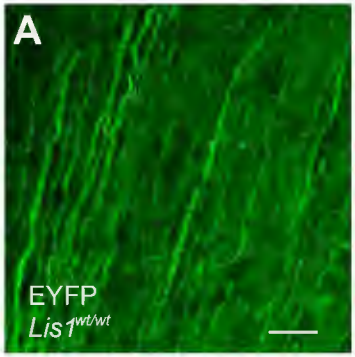
A
EYFP
Lis1wt/wt

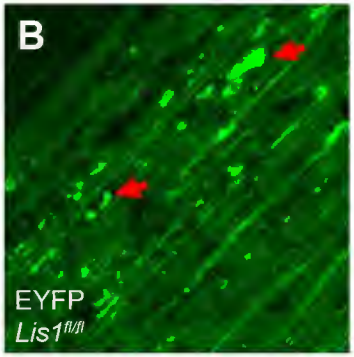
B
EYFP
Lis1fl/fl

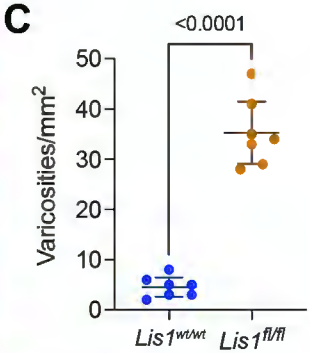
C
<0.0001
Varicosities/mm2
50
40
30
20
10
0
Lis1wt/wt
Lis1fl/fl

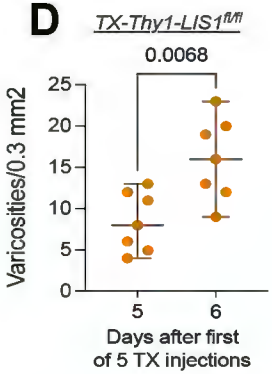
D
TX-Thy1-LIS1fl/fl
0.0068
Varicosities/0.3 mm2
25
20
15
10
5
0
5
6
Days after first
of 5 TX injections

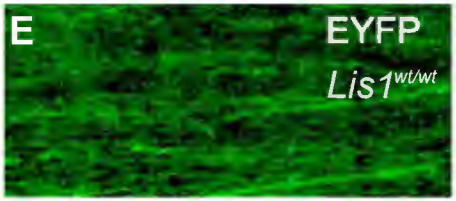
E
EYFP
Lis1wt/wt

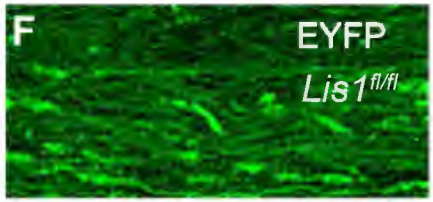
F
EYFP
Lis1fl/fl

DegenoTag

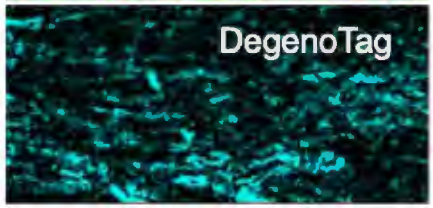
DegenoTag

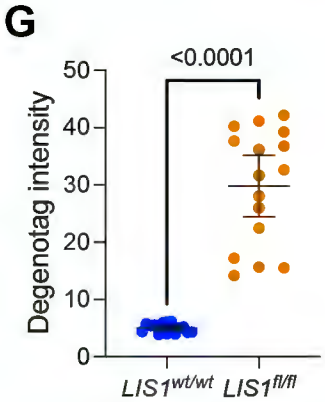
G
<0.0001
Degenotag intensity
50
40
30
20
10
0
LIS1wt/wt
LIS1fl/fl

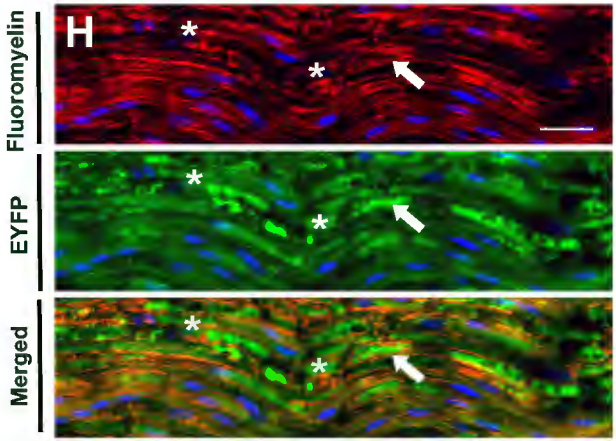
H
Fluoromyelin
EYFP
Merged

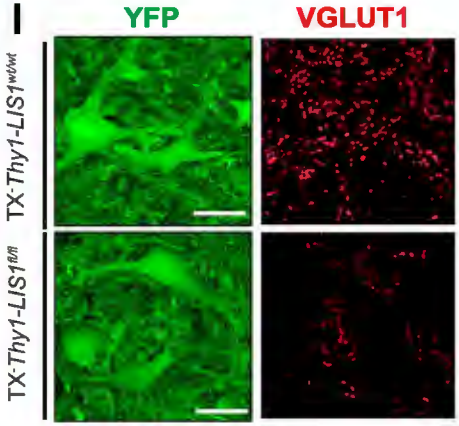
I
YFP
VGLUT1
TX-Thy1-LIS1wt/wt
TX-Thy1-LIS1fl/fl

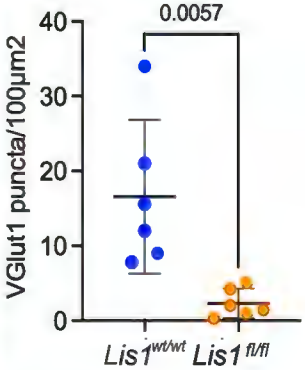
J
0.0057
VGlut1 puncta/100µm2
40
30
20
10
0
Lis1wt/wt
Lis1fl/fl

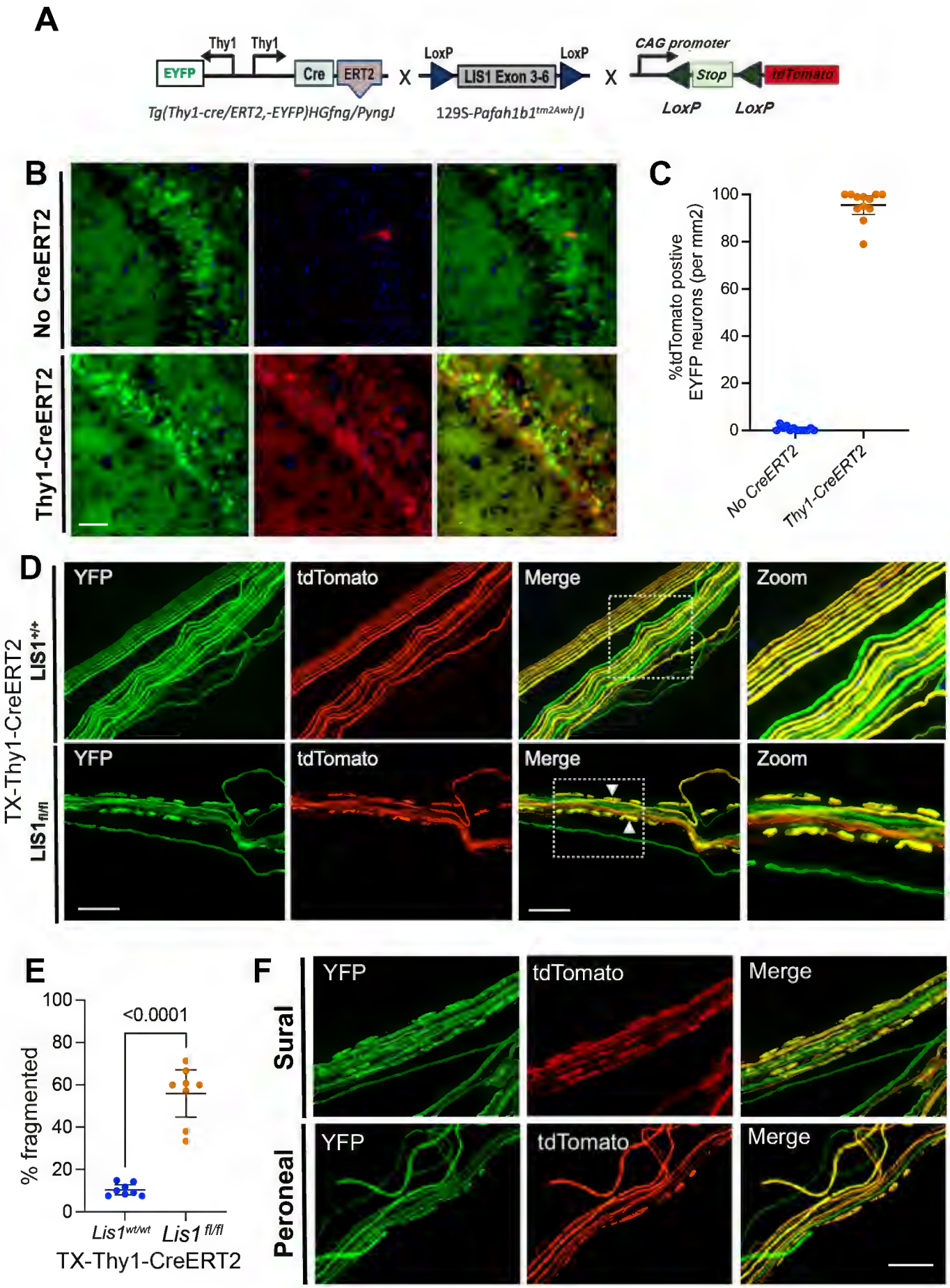
A
Thy1
Thy1
EYFP
Cre
ERT2
X
LoxP
LIS1 Exon 3-6
LoxP
X
CAG promoter
Stop
tdTomato
Tg(Thy1-cre/ERT2,-EYFP)HGfng/PyngJ
129S-Pafah1b1tm2Awb/J
LoxP
LoxP
B
No CreERT2
Thy1-CreERT2
C
%tdTomato postive EYFP neurons (per mm2)
100
80
60
40
20
0
No CreERT2
Thy1-CreERT2
D
TX-Thy1-CreERT2
LIS1+/+
LIS1fl/fl
YFP
tdTomato
Merge
Zoom
YFP
tdTomato
Merge
Zoom
E
% fragmented
100
80
60
40
20
0
<0.0001
Lis1wt/wt
Lis1 fl/fl
TX-Thy1-CreERT2
F
Sural
Peroneal
YFP
tdTomato
Merge
YFP
tdTomato
Merge

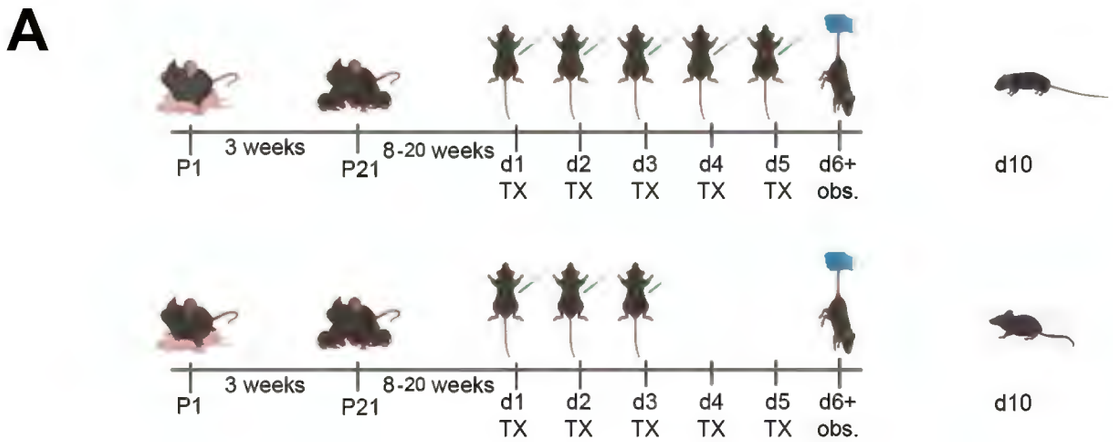

B

5 TX inj.

	TX-Thy1-LIS1 wt/wt (N = 26)	*TX-Thy1-LIS1 fl/fl* (N = 38)
Leg clasping	0	38
Altered gait	0	38
Seizures/shivering	0	38
Weight loss	0	38

3 TX inj.

	TX-Thy1-LIS1 wt/wt (N = 12)	*TX-Thy1-LIS1 fl/fl* (N = 12)
Leg clasping	0	12
Altered gait	0	12
Seizures/shivering	0	0
Weight loss	0	0

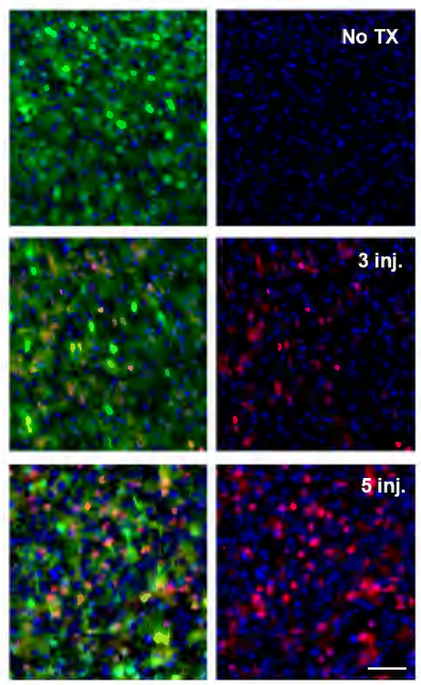

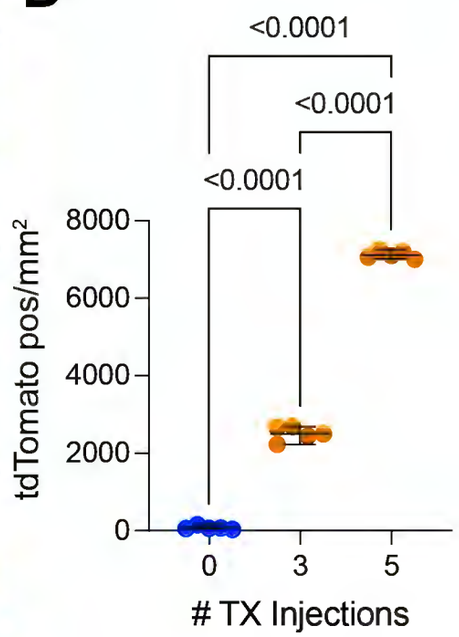

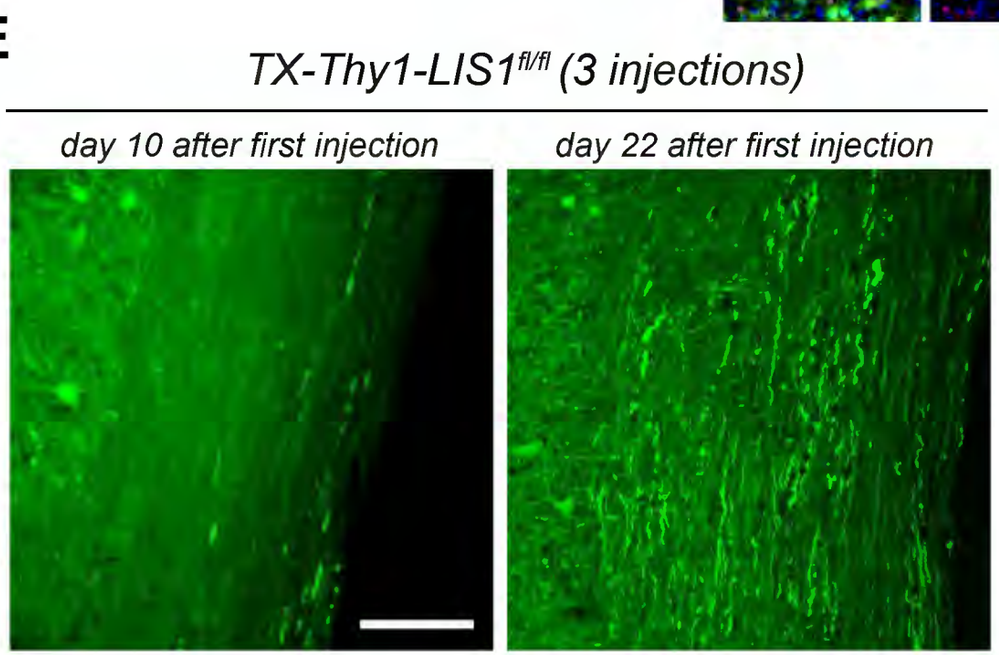

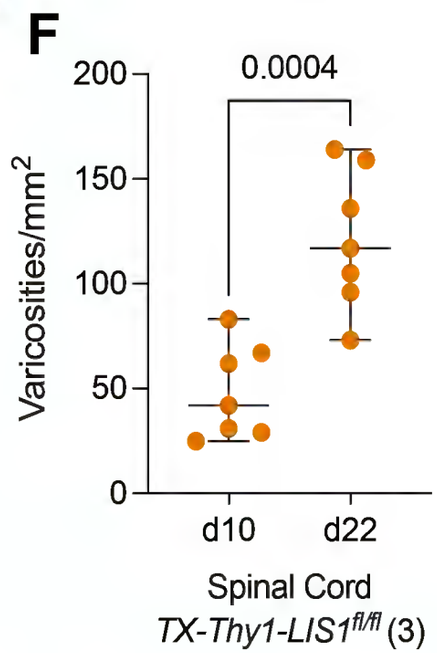

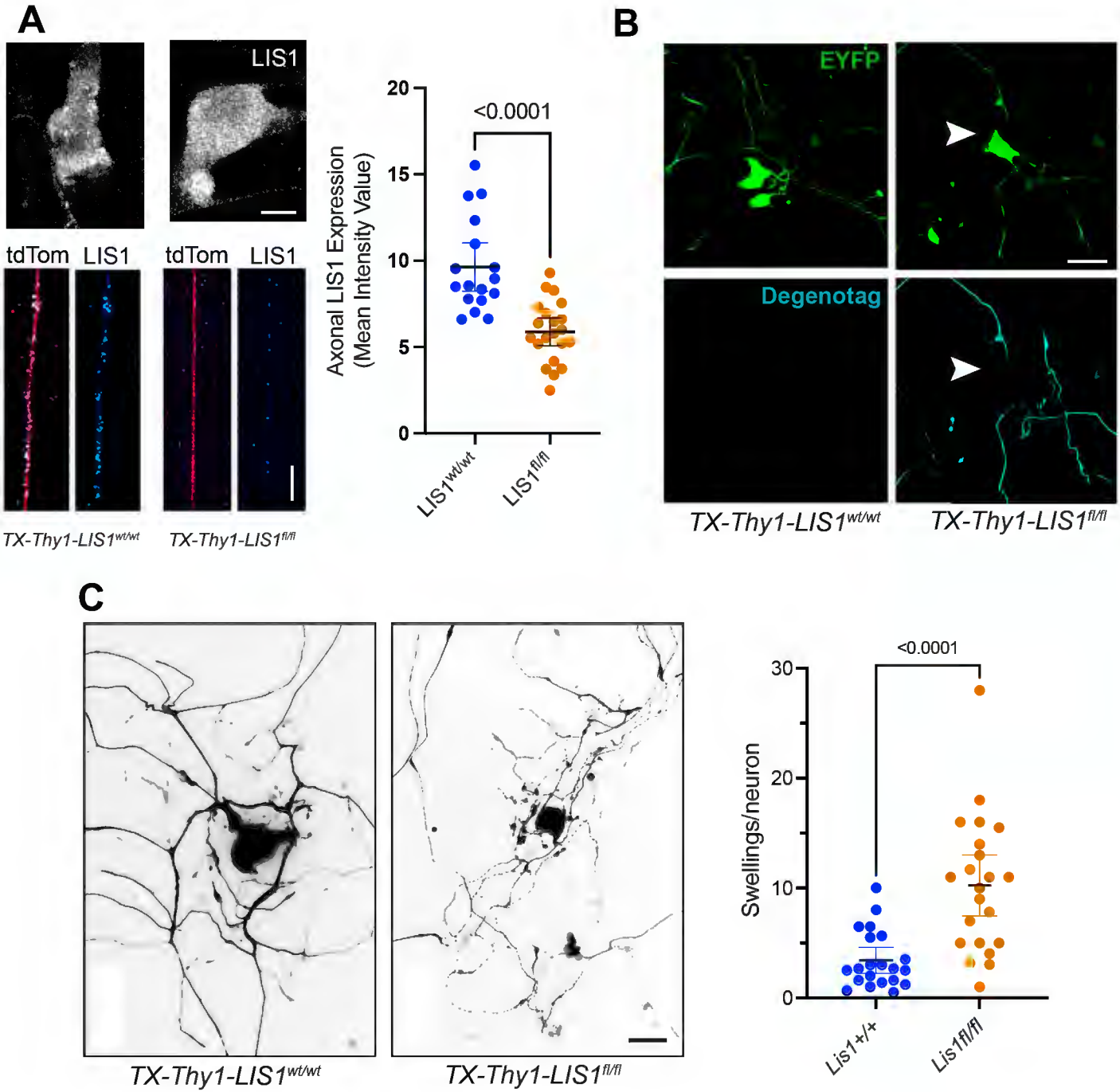
A
LIS1
tdTom
LIS1
tdTom
LIS1
TX-Thy1-LIS1wt/wt
TX-Thy1-LIS1fl/fl
<0.0001
Axonal LIS1 Expression
(Mean Intensity Value)
20
15
10
5
0
LIS1wt/wt
LIS1fl/fl
B
EYFP
Degenotag
TX-Thy1-LIS1wt/wt
TX-Thy1-LIS1fl/fl
C
TX-Thy1-LIS1wt/wt
TX-Thy1-LIS1fl/fl
<0.0001
Swellings/neuron
30
20
10
0
Lis1+/+
Lis1fl/fl